Disruption of *Mtmr2* produces CMT4B1-like neuropathy with myelin outfolding and impaired spermatogenesis

Alessandra Bolino,[1] Annalisa Bolis,[1] Stefano Carlo Previtali,[2] Giorgia Dina,[2] Simona Bussini,[1] Gabriele Dati,[3] Stefano Amadio,[2] Ubaldo Del Carro,[2] Dolores D. Mruk,[4] Maria Laura Feltri,[3] C. Yan Cheng,[4] Angelo Quattrini,[2] and Lawrence Wrabetz[3]

[1]Dulbecco Telethon Institute, [2]Department of Neurology, and [3]Department of Biological and Technological Research, San Raffaele Scientific Institute, 20132 Milan, Italy
[4]Population Council, Center for Biomedical Research, The Rockefeller University, New York, NY 10021

Mutations in *MTMR2*, the myotubularin-related 2 gene, cause autosomal recessive Charcot-Marie-Tooth (CMT) type 4B1, a demyelinating neuropathy with myelin outfolding and azoospermia. *MTMR2* encodes a ubiquitously expressed phosphatase whose preferred substrate is phosphatidylinositol (3,5)-biphosphate, a regulator of membrane homeostasis and vesicle transport. We generated *Mtmr2*-null mice, which develop progressive neuropathy characterized by myelin outfolding and recurrent loops, predominantly at paranodal myelin, and depletion of spermatids and spermatocytes from the seminiferous epithelium, which leads to azoospermia. Disruption of *Mtmr2* in Schwann cells reproduces the myelin abnormalities. We also identified a novel physical interaction in Schwann cells, between Mtmr2 and discs large 1 (Dlg1)/synapse-associated protein 97, a scaffolding molecule that is enriched at the node/paranode region. Dlg1 homologues have been located in several types of cellular junctions and play roles in cell polarity and membrane addition. We propose that Schwann cell–autonomous loss of Mtmr2–Dlg1 interaction dysregulates membrane homeostasis in the paranodal region, thereby producing outfolding and recurrent loops of myelin.

Introduction

The myotubularins are part of the phosphotyrosine phosphatase/dual specificity phosphatase (PTP/DSP) super family. There are 14 members in humans, named myotubularin (MTM) 1 and myotubularin-related protein (MTMR) 1–13, including both catalytically active and inactive enzymes. MTM1 is mutated in X-linked myotubular myopathy, a severe congenital muscular disorder (Laporte et al., 2003). Myotubularins all share four domains: GRAM (glucosyltransferase, Rab-like GTPase activators, and myotubularins), RID (Rac-induced recruitment domain), PTP/DSP, and SID (SET motif–interacting domain). A coiled-coil domain is located at the COOH terminus of most myotubularins. Domains found in a subset of myotubularins, such as FYVE (Fab1p, YO1B, Vac1p, and EEA1) and pleckstrin homology domains, are associated with phosphoinositide and membrane trafficking. Also, a PDZ (PSD-95/Dlg/ZO-1)–binding site is present in five MTMRs, including MTMR2 and MTMR13, both of which are mutated in Charcot-Marie-Tooth (CMT) disease type 4B (Laporte et al., 2003).

CMT neuropathies, associated with 21 genes, are characterized by progressive muscular atrophy and weakness in the distal extremities (for review see Suter and Scherer, 2003; http://www.molgen.ua.ac.be/CMTMutations/default.cfm). The autosomal recessive CMT4B manifests as childhood onset of weakness and sensory loss, severely decreased nerve conduction velocity, and demyelination with myelin outfoldings in the peripheral nerve (Quattrone et al., 1996). Putative loss of function mutations have been described in either *MTMR2* (CMT4B1) or *MTMR13* (CMT4B2) (Bolino et al., 2000; Houlden et al., 2001; Azzedine et al., 2003; Senderek et al., 2003). MTMR2 and MTMR13 are catalytically active and inactive enzymes, respectively, that are both ubiquitously expressed (Berger et al., 2002; Bolino et al., 2002; Azzedine et al., 2003). One CMT4B1 patient manifested azoospermia (Laporte et al.,

Correspondence to Alessandra Bolino: bolino.alessandra@hsr.it

Abbreviations used in this paper: CMT, Charcot-Marie-Tooth; CMV, cytomegalovirus; MAG, myelin-associated glycoprotein; MAGUK, membrane-associated guanylate kinase-like; MTM, myotubularin; MTMR, myotubularin-related protein; PDZ, PSD-95/Dlg/ZO-1; PtdIns3,5P2, phosphatidylinositol (3,5)-biphosphate; PTP/DSP, phosphotyrosine phosphatase/dual specificity phosphatase.

The Journal of Cell Biology, Vol. 167, No. 4, November 22, 2004 711–721
http://www.jcb.org/cgi/doi/10.1083/jcb.200407010

2003), which suggests that MTMR2 also plays an important role in the testis, where its expression is enriched (Li et al., 2000).

Although MTMRs share extensive homology with PTP/DSP phosphatases, they preferentially dephosphorylate phosphoinositides (Laporte et al., 2003). The likely physiological substrate of both MTM1 and MTMR2 is phosphatidylinositol (3,5)-biphosphate (PtdIns3,5P2; Berger et al., 2002, 2003; Tsujita et al., 2004), a key regulator of vacuolar homeostasis and vesicle transport at the level of multivesicular bodies/late endosomes (Odorizzi et al., 1998; Ikonomov et al., 2002). Hence, MTMR2 may regulate membrane transport, which is crucially important in both neurons and Schwann cells. Recently, we found that Mtmr2 is expressed in all cells within the peripheral nerve, including neurons, their axons, and all of the cytoplasmic spaces of myelin-forming Schwann cells. In neurons, MTMR2 may interact with NF-L (neurofilament light chain protein), a nervous system–specific protein mutated in axonal CMT2E. NF-L might recruit and concentrate MTMR2 phosphatase to its site of action, where subpools of phosphoinositides may be localized (Previtali et al., 2003). In Schwann cells, the role of MTMR2, and whether or not its loss produces myelin outfoldings, is unknown.

To address these questions, we generated mice with *Mtmr2* inactivated either in all cells or only in Schwann cells. *Mtmr2*-null mice display a motor and sensory peripheral neuropathy with myelin outfoldings, as well as defects in spermatogenesis, thus reproducing the CMT4B1 pathology. Schwann cell–specific inactivation of *Mtmr2* reproduces the myelin alterations seen in the complete *Mtmr2*-null mice. Interestingly, folds and recurrent loops of myelin arise predominantly from paranodal regions, after paranodal architecture is already established. We also report that Mtmr2 interacts with discs large 1/synapse-associated protein 97 (Dlg1/SAP97), a PDZ-domain containing scaffolding molecule of the membrane-associated guanylate kinase-like (MAGUK) protein family that has not been described previously in Schwann cells (Humbert et al., 2003). Dlg1 is detected in the cytoplasm of Schwann cells and in noncompact myelin, including paranodes and microvilli, where it is enriched. Dlg1 localization is altered in *Mtmr2*-null Schwann cells. We propose that loss of interaction between Dlg1 and Mtmr2 dysregulates cellular junctions or membrane remodelling in Schwann cells, thereby provoking myelin outfoldings at the paranodes.

Results

Disruption of *Mtmr2*

To generate a conditional *Mtmr2*-null allele, we flanked exon 4 with *lox-P* sites, because its excision introduces a frameshift from either ATG start site of translation (exon 1 or 3); virtual translation predicts a short peptide without putative functional domains (Fig. 1 A). In addition, a naturally occurring nonsense mutation in exon 4, thought to produce complete loss of function, was described in an Indian family with typical CMT4B1 (Houlden et al., 2001). The *Mtmr2*-null allele was produced by crossing *Mtmr2*-floxed mice with *cytomegalovirus* (*CMV*) *promoter–Cre* transgenic mice. The deletion of exon 4 was docu-

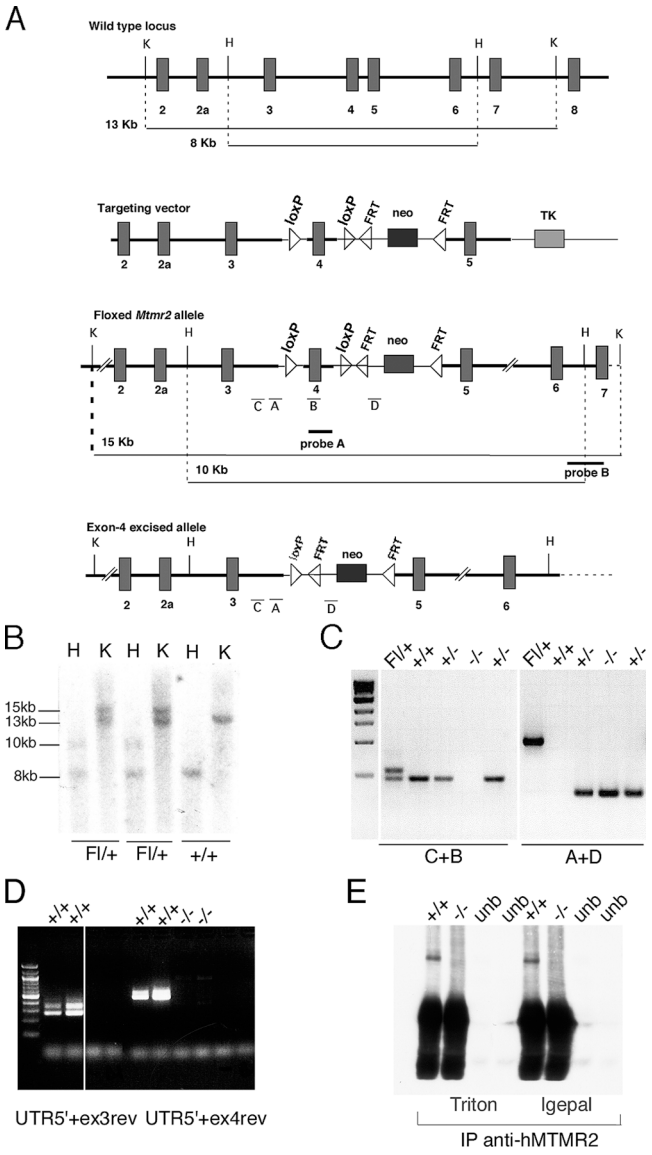

Figure 1. **Generation of the *Mtmr2*-null allele.** (A) Schematic diagrams (from top) show the following: genomic structure of *Mtmr2* surrounding exon 4 (wild-type locus); targeting construct where genomic *Mtmr2* fragments are indicated with thick lines and vector-derived segments with thin lines (targeting vector); the *Mtmr2* locus after homologous recombination in embryonic stem cells (floxed *Mtmr2* allele); the floxed *Mtmr2* allele after *CMV-Cre*–mediated excision of exon 4 (exon 4 excised allele). The KpnI (K) and HindIII (H) restriction sites, as well as probes used for Southern blot analysis, are shown. A–D are primers used for genotype analysis. (B) Southern blot analysis of embryonic stem cell clones containing the targeted (floxed, *Fl/+*) allele after homologous recombination. DNA was digested with KpnI (K) and HindIII (H) and hybridized with probe A. The last two lanes (+/+) contain DNA from wild-type embryonic stem cells. (C) Genotyping of mouse tail DNA using primer pairs C + B and A + D. (+/+) is a wild-type mouse; (*Fl/+*) is a mouse carrying the targeted floxed allele, before *CMV-Cre*–mediated excision of exon 4; (+/−) is a heterozygous mouse for the *CMV-Cre*–mediated excision of exon 4; and (−/−) is a homozygous null mouse where the excision of exon 4 occurred on both *Mtmr2* alleles. (D) RT-PCR analysis on sciatic nerve mRNA from wild-type (+/+) and *Mtmr2*-null animals (−/−). When a reverse primer recognizing exon 4 was used, no amplification was detected in *Mtmr2* (−/−) mice. cDNA synthesis was performed using both oligo-dT and random hexamers on total RNA from wild-type and mutant nerves. (C and D) White lines indicate that intervening lanes have been spliced out. (E) Western blot analysis of Mtmr2 immunoprecipitated using anti-hMTMR2 antibodies. Brain homogenates from wild-type (+/+) and mutant (−/−) animals were prepared using two different lysis buffers containing either Igepal or Triton X-100 as detergents. Unb, unbound fraction after immunoprecipitation.

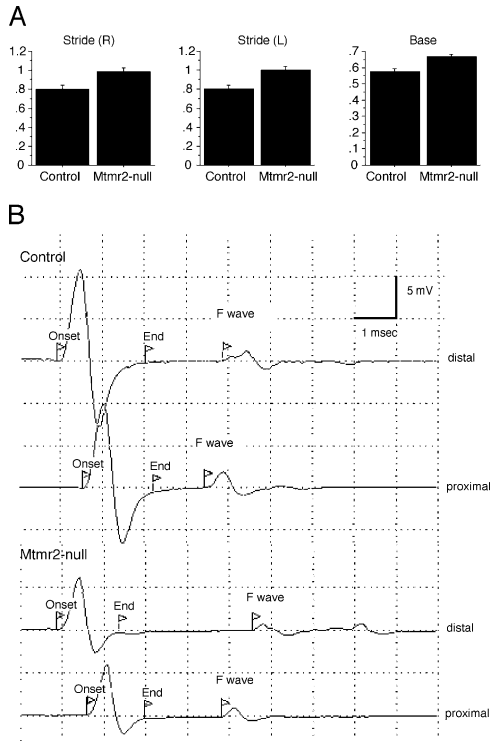

Figure 2. **Gait and electrophysiological analysis of *Mtmr2*-null mice.** (A) Gait analysis revealed that right stride (R) ($F[1, 18] = 9.96$; $P = 0.0055$); left stride (L) ($F[1, 18] = 10.97$; $P = 0.0039$); and base ($F[1, 18] = 16.746$; $P = 0.0007$) were significantly increased in mutant mice as compared with wild-type mice, at 6 mo old. Values on the y axis refer to the measures normalized for the length of the animals (from the nape of the neck to the insertion of the tail). (B) Traces show the control and *Mtmr2*-null profiles of compound motor action potential recorded after stimulation at the ankle (distal) and at the sciatic notch (proximal). The onset and end of the compound motor action potential and the onset of the F-wave are indicated by flags.

mented in progeny by PCR analysis of genomic DNA (Fig. 1 C). Heterozygous *Mtmr2* exon 4–deleted mice were crossed to generate *Mtmr2* homozygous null mice. No *Mtmr2* mRNAs containing exon 4 or 3′-exons could be detected by RT-PCR analysis of total RNA from the tail, brain, muscle, and sciatic nerve (Fig. 1 D and not depicted). Immunoprecipitation followed by Western blot analysis revealed that Mtmr2 protein was absent from brain lysates in *Mtmr2*-null animals (Fig. 1 E).

Mtmr2 (−/−) mice are viable, but *Mtmr2*-null animals were underrepresented (29 out of 205 animals, or 14% [vs. the expected 25%]). *Mtmr2*-null mice weighed less than wild-type littermates, at all ages (18.7 ± 0.8 g(3) vs. 22 ± 1.2 g(5); $P <$ 0.01 in males at 1 mo old, for example; mean ± SEM(n); t test), as described previously for *Mtm1*-null mice (Buj-Bello et al., 2003). Most *Mtmr2*-null mice appeared otherwise normal, although they occasionally showed mild tremor and signs of functional disability, such as widely placed hindpaws and clenching of the paws when suspended by the tail.

Behavioral and neurophysiological analysis

At 6 mo old, *Mtmr2*-null animals and wild-type littermates showed no significant difference on rotarod testing (not depicted). Instead, gait analysis revealed significantly wider base and longer stride in *Mtmr2*-null mice (Fig. 2 A), suggesting a neuromuscular abnormality. Consistent with this, *Mtmr2*-null mice also showed reduced nerve conduction velocities ($30.8 \pm 0.8(8)$ m/s vs. $38.7 \pm 0.5(20)$ m/s, $P \ll 0.001$) and prolonged F-wave latencies ($5.30 \pm 0.13(8)$ ms vs. $4.99 \pm 0.04(20)$ ms, $P <$ 0.005). The amplitudes of proximal and distal compound motor action potentials were normal (Fig. 2 B). These findings are consistent with a peripheral neuropathy in *Mtmr2*-null mice.

Peripheral neuropathy in *Mtmr2*-null mice

Necropsy of *Mtmr2*-null mice revealed normally formed organs without obvious abnormality. Histology of the brain, spinal cord, and muscle (including ATPase isotype staining) was grossly normal at 2 mo old. Only peripheral nerves demonstrated abnormalities (Fig. 3 and not depicted). The predominant changes were seen in myelin sheaths; transverse semithin sections revealed myelin outfolding that appeared as "comma"-shaped extensions of both myelin and axoplasm (Figs. 3 E and 4 A), or recurrent loops that appeared as one to five satellite myelinated axons around a larger myelinated axon (Fig. 3, E and M; and Fig. 4, B and C). Less frequently, myelin protruded into the axon, producing a myelinated fiber within a larger myelinated axon (Figs. 3 E and 4 B). The number of fibers containing myelin outfoldings and loops increased progressively in sciatic nerves of null mice examined at 1 mo (4.1%), 2 mo (5.2%), 4 mo (7.7%), and 6 mo old (11%; Fig. 3, compare E with F). The complexity of myelin outfoldings also progressed with age, because the number of fibers showing three or more satellite loops increased from 2.5% at 1 mo to 6.25% at 2 mo, 10% at 4 mo, and 8.4% at 6 mo old. Almost all large myelinated fibers in digital nerves of null mice contained myelin outfoldings (Fig. 3 O), suggesting that the morphological alterations were length dependent.

To determine whether both motor and sensory nerves were affected as in CMT4B1, we examined quadriceps and saphenous nerves, respectively, from *Mtmr2* (−/−) mice. Myelin outfoldings were obvious in transverse sections of both (Fig. 3, J–M). In addition, at 6 mo old in sciatic nerve, occasional degenerating axons were seen, although without evident onion bulbs, which would suggest preceding demyelination (unpublished data). Overall, the dysmyelinating phenotype of *Mtmr2*-null mice is remarkably similar to that of CMT4B1 neuropathy (for comparison see Houlden et al., 2001).

To determine when and where myelin outfoldings arise along fibers, we examined nerves of *Mtmr2*-null mice during the formation of myelin internodes in the 3 wk after birth. Sciatic nerves from *Mtmr2*-null mice at P19 appeared normal with no signs of dysmyelination (unpublished data), suggesting that myelin outfoldings first appear between 3 and 4 wk after birth, a period when the architecture of the myelin internode is already well-established (Webster, 1971). Serial transverse semithin sections of *Mtmr2*-null sciatic nerves demonstrated that many recurrent loops of myelin extend from the level of the nodes of Ranvier backward, toward the Schwann cell nucleus, roughly parallel to the internode (Fig. 3, A–D). Moreover, longitudinal semithin sections of mutant nerves revealed that

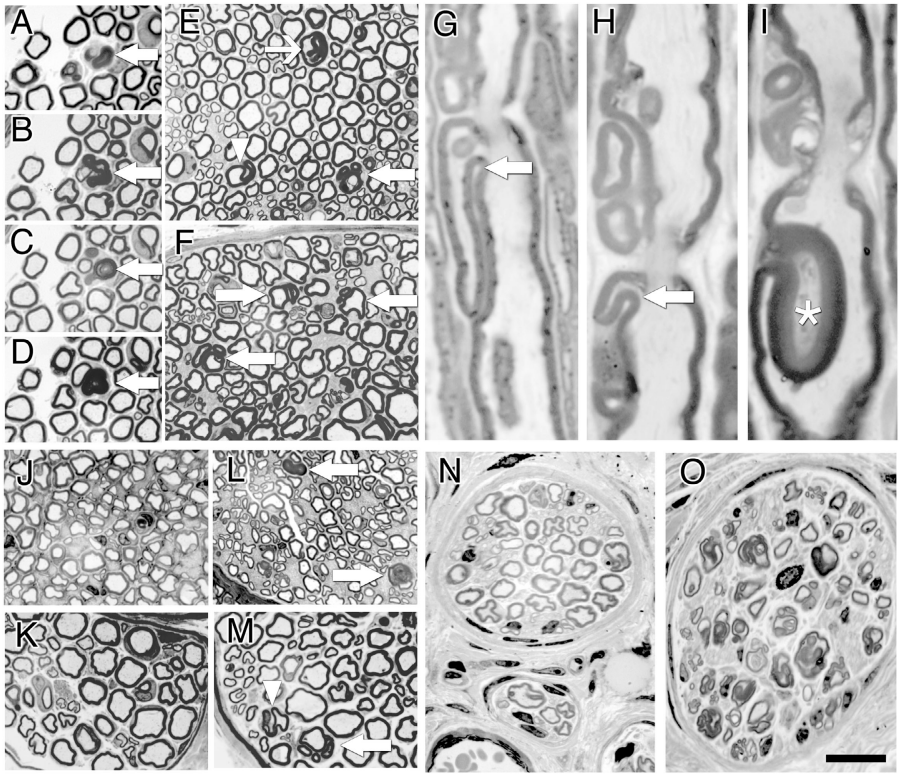

Figure 3. **Myelin outfoldings in *Mtmr2*-null peripheral nerves.** (A–D) Serial transverse sections of *Mtmr2*-null sciatic nerves at 4 wk old. Arrows indicate a fiber with myelin outfoldings extending from the node (A) throughout the internode (B–D). (E and F) Transverse sections of mutant sciatic nerves at 7 wk (E) and 6 mo old (F), where arrows indicate myelin outfoldings; open arrow (E) indicates a myelin infolding, and the arrowhead indicates a comma-shaped myelin outfolding. (G–I) Longitudinal sections of sciatic nerves from *Mtmr2*-null mice, where arrows indicate the onset of myelin outfoldings and recurrent loops at the paranodes/juxtaparanodes. The asterisk marks a loop of Schwann cell membrane protruding into the axonal space (infolding). (J–M) Cross sections of saphenous nerves from a wild-type (J) and a mutant (L) mouse, or quadriceps nerves from a wild-type (K) and a (M) mutant mouse. Myelin outfoldings are evident (L and M, arrows) in both mutant nerves; the arrowhead indicates a comma-shaped myelin outfolding. (N and O) Cross sections of digital nerves from a wild-type (N) or a mutant (O) mouse, where myelin outfoldings are present in almost all myelinated fibers. Bar: (A–F and J–O) 15 μm; (G–I) 5 μm.

many myelin outfoldings/infoldings and recurrent loops were predominant near, and probably arose from, juxtaparanodal/paranodal regions (Fig. 3, G–I).

Electron microscopic analysis of sciatic nerves from *Mtmr2* (−/−) animals at 7 wk old showed that the compaction and periodicity of myelin appeared normal, suggesting that the molecular architecture of compact myelin was not impaired. Also, Schwann cells (with or without recurrent loops) displayed a normal basal lamina at their ab-axonal surfaces (Fig. 4, A–D). Non–myelin-forming Schwann cells appeared normal. Electron microscopy of longitudinal sections confirmed that the complex loops and folding of myelin were predominant around the paranode and extended along the adjacent internode (Fig. 4 D). Counting myelin outfolds/loops with axoplasm contiguous with the central axon revealed that only 2 out of 30 internodal segments had outfolds, whereas 16 out of 17 nodes had at least one fold within 10 μm of the paranode.

Expression analysis in *Mtmr2*-null sciatic nerves

To assess whether absence of Mtmr2 altered myelin protein levels, we performed Western blot analysis on sciatic nerve homogenates. PMP-22 (peripheral myelin protein 22) and P0 (myelin protein zero) levels were normal in *Mtmr2*-null sciatic nerves (Fig. 5 Z), in keeping with the normal compaction and periodicity of myelin. On the other hand, the level of myelin-associated glycoprotein (MAG) was decreased in *Mtmr2*-null sciatic nerves, an observation that is consistent with an alteration in noncompact myelin (mesaxonal loops, incisures, or paranodal loops; Fig. 5 Z). We also investigated whether expression of NF-L, an interactor of Mtmr2 in both axons and

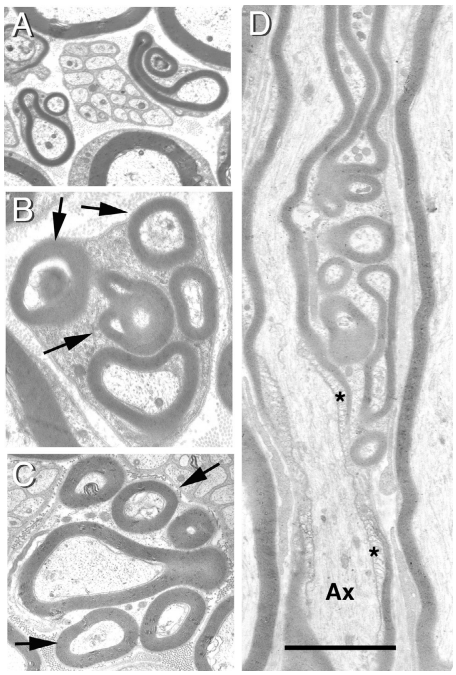

Figure 4. **Ultrastructural analysis of *Mtmr2*-null sciatic nerves.** (A–C) Transverse sections of *Mtmr2*-null sciatic nerves. (A) Comma-shaped myelin foldings and recurrent loops are seen in myelin-forming Schwann cells, whereas non–myelin-forming Schwann cells appear normal (center of section). (B–D) A normal basal lamina wraps myelin outfoldings. (B and C) Arrows indicate satellite myelinated axons around a larger myelinated axon. (D) Longitudinal section of a mutant sciatic nerve in which the myelin outfoldings originate at the paranode and extend along the internode. Asterisks mark paranodal loops in contact with axons; the gross architecture of axoglial contacts is preserved in *Mtmr2*-null mouse fibers. Ax, axon. The node of Ranvier is located between the two asterisks. Bar: (A) 4 μm; (B–D) 3 μm.

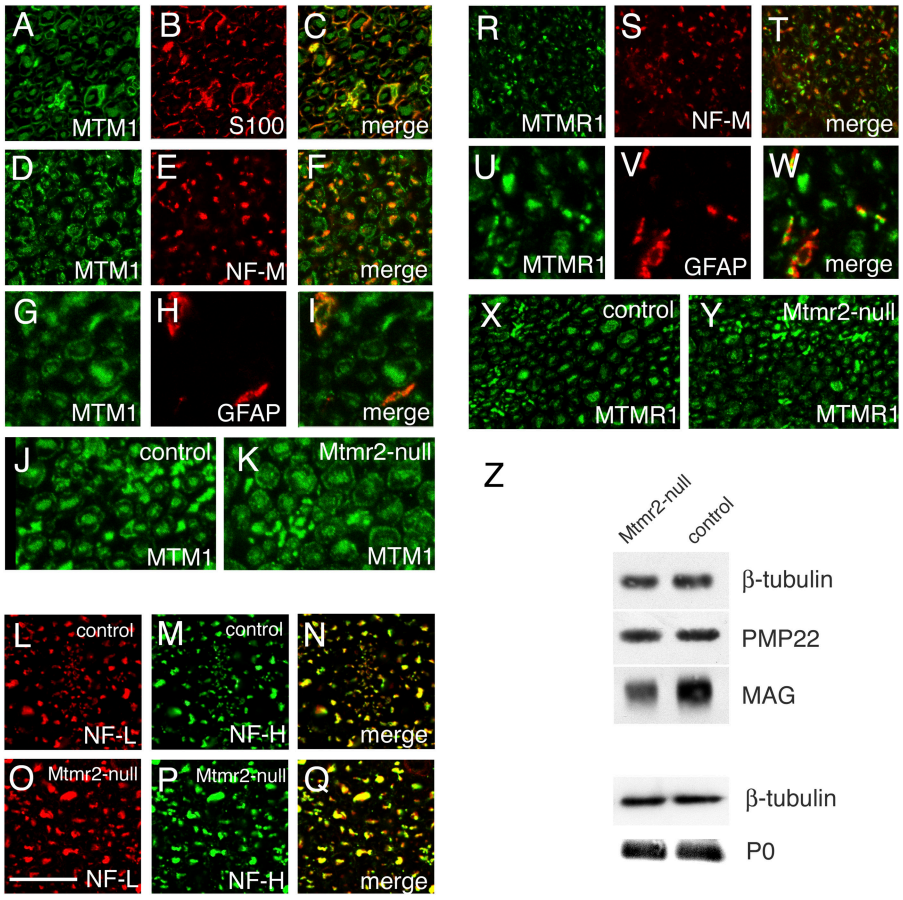

Figure 5. **Expression analysis in *Mtmr2*-null sciatic nerve.** (A–I) Immunohistochemical localization of Mtm1 in rat sciatic nerve using anti-Mtm1 polyclonal antibodies (A, D, and G). Mtm1 is located in the cytoplasm of myelin-forming Schwann cells, as shown by double staining with S100 (A–C); in axons, as shown by double staining with NF-M (D–F); and in non–myelin-forming Schwann cells, as revealed by double staining with GFAP (G–I). Immunohistochemical localization of Mtm1 was similar in sciatic nerves from control (J) and *Mtmr2*-null (K) mice. (L–Q) Immunostaining for NF-L in mouse sciatic nerves from control (L–N) and *Mtmr2*-null mice (O–Q). NF-H staining revealed all axons in normal (M) and mutant (P) mouse nerves. (R–W) Immunohistochemical localization of Mtmr1 in rat sciatic nerves using anti-Mtmr1 antibodies. Mtmr1 is localized in axons (R–T) and in the cytoplasm of non–myelin-forming Schwann cells (U–W). Mtmr1 was not detected in the cytoplasm of myelin-forming Schwann cells. No difference in Mtmr1 staining was observed between wild-type (X) and *Mtmr2*-null (Y) sciatic nerves. (Z) Western blot analysis of P0, PMP-22, and MAG on sciatic nerve homogenates from normal and mutant animals. β-Tubulin was used to normalize loading. Bar: (A–F and L–T) 32 μm; (G–I and V and W) 20 μm; and (J, K, X, and Y) 25 μm.

denervated Schwann cells (Previtali et al., 2003), was altered in sciatic nerves from *Mtmr2*-null mice. The pattern and intensity of the NF-L immunostaining, as well as its level, were similar in mutant and wild-type nerves (Fig. 5, L–Q; and not depicted). NF-H immunostaining also appeared normal in mutant nerves (Fig. 5 P). Thus, loss of Mtmr2 does not seem to affect neurofilament expression or assembly in axons.

To determine possible compensation or redundancy in the absence of Mtmr2, we stained nerves for Mtm1 and Mtmr1, which are both highly homologous to Mtmr2. In normal rat sciatic nerve, two different antibodies against Mtm1 revealed expression in the cytoplasms of both myelin-forming and non–myelin-forming Schwann cells, as well as in axons, all of which are locations where Mtmr2 is also expressed (Fig. 5, A–I; Previtali et al., 2003). On the contrary, an antibody against Mtmr1 revealed staining in the cytoplasm of non–myelin-forming Schwann cells and in axons, but not in myelin-forming Schwann cells (Fig. 5, R–W). Each of the Mtm1 or Mtmr1 antibodies produced similar patterns and intensities of staining on *Mtmr2* (−/−) and control sciatic nerves (Fig. 5, J, K, X, and Y). These findings suggest that loss of Mtmr2 does not significantly affect the expression of Mtm1 and Mtmr1. It is important to note the difficulty of using antibodies to MTMR family members in mouse nerve. Two different antibodies against human MTMR2 and one against rat Mtmr2 all produced a positive staining in the cytoplasm of both Schwann cells and axons in *Mtmr2*-null nerves, where *Mtmr2* was absent in null animals as shown by RT-PCR analysis and by immunoprecipitation followed by Western blot analysis (Fig. 1 D). However, these same antibodies produced no staining on frozen sural nerve biopsies of CMT4B1 patients (unpublished data), and produced staining in all cytoplasmic spaces of Schwann cells and axons in control human nerves (Fig. 6, J–L; Previtali et al., 2003). Thus, in immunohistochemistry, it is possible that Mtmr2 antibodies also recognize an MTMR2 homologue in mouse nerves that is distributed similarly to Mtmr2.

Schwann cell–specific inactivation of *Mtmr2* produces myelin outfoldings

We have provided evidence that Mtmr2 interacts with NF-L in axons (Previtali et al., 2003), where it may serve to transport and localize the phosphatase to a particular subcellular domain. However, this interaction does not account for a cell-autonomous role for Mtmr2 in myelin-forming Schwann cells, even if one is strongly suggested by the myelin alterations in humans and mice with loss of Mtmr2 function. To address this, we crossed the *Mtmr2*-floxed mice with P0-Cre mice. P0-Cre produces somatic recombination of floxed genes only in Schwann cells and not in dorsal root or spinal motor neurons that contribute axons to peripheral nerves (Feltri et al., 2002). In situ hybridization and RT-PCR analysis for *Mtmr2* mRNA, together with a PCR-based recombination assay on genomic DNA from P0-Cre/*Mtmr2* (Fl/Fl) mice, showed that the majority of *Mtmr2* was excised specifically in peripheral nerves; the

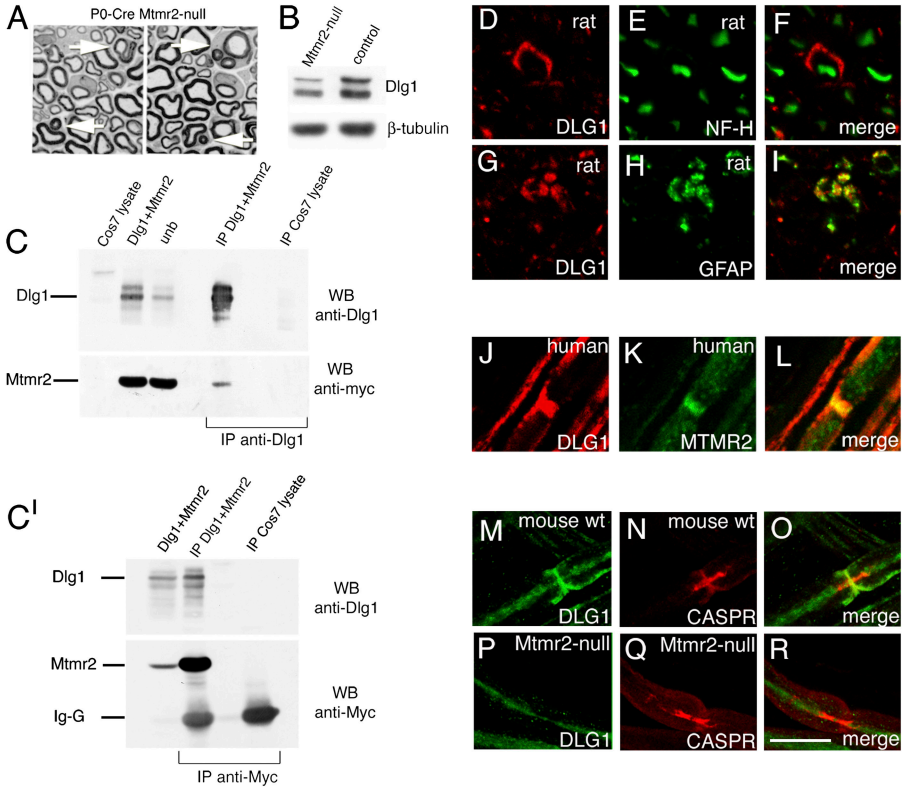

Figure 6. **Mtmr2 interacts with Dlg1/SAP97.** (A) Semithin section analysis of sciatic nerves from mutant mice with conditional ablation of *Mtmr2* in Schwann cells (P0-Cre/Mtmr2-null) demonstrate myelin outfoldings (arrows). (B) Western blot analysis for Dlg1 in sciatic nerve homogenates from wild-type and *Mtmr2*-null animals. β-Tubulin was used to normalize loading. (C) Coimmunoprecipitation of Mtmr2-Myc and Dlg1. Mtmr2-Myc was detected in immunoprecipitates prepared from lysates of COS-7 cells cotransfected with Dlg1 and Mtmr2-Myc (IP Dlg1 + Mtmr2) but not in untransfected cells (IP COS-7 lysate). Lanes (from left) show the following: untransfected COS-7 cells; cells cotransfected with both Dlg1 and Mtmr2-Myc; unbound fraction of the immunoprecipitation performed with anti-Dlg1 antibody on the lysates of cotransfected cells; immunoprecipitation from cotransfected cells performed with anti-Dlg1 antibody; and immunoprecipitation from untransfected cells. (C′) Converse coimmunoprecipitation in which an anti-Myc antibody was used to immunoprecipitate Mtmr2-Myc bound to Dlg1, as revealed by Western blot using an anti-Dlg1 antibody. (D–I) Immunohistochemistry on rat sciatic nerves using anti-Dlg1 antibody (D and G); anti–NF-H antibody to recognize axons, where Dlg1 is detected in a ring at the ab-axonal surface of a myelin-forming Schwann cell (F); and anti-GFAP to recognize non–myelin-forming Schwann cells (H), showing that Dlg1 is also expressed there (I). (J–L) MTMR2 is enriched at nodal regions of Schwann cells in human fibers stained with anti-hMTMR2 antibody (K) and colocalizes with DLG1 there (J and L). (M–O and P–R) Costaining of DLG1 and CASPR, which identifies paranodal domains, in teased fibers from normal (M) and *Mtmr2*-null (P) mice. Dlg1 is enriched in the nodal–paranodal domain of normal fibers (M). This enrichment was much less obvious on fibers from mutant animals (P). Bar: (D–F and J–R) 12 μm; (G–I) 16 μm.

remaining unexcised *Mtmr2* probably derives from perineurial cells (unpublished data). Sciatic nerves from P0-Cre/*Mtmr2* (Fl/Fl) mice revealed myelin outfoldings and recurrent loops in similar numbers (in transverse semithin sections, 5% of myelinated fibers at 2 mo, 10% at 4 mo, and 16% at 6 mo old) and location as seen in *Mtmr2*-null mice (compare Fig. 6 A with Fig. 3, E and F).

Mtmr2 interacts with Dlg1 in Schwann cells

To identify a Schwann cell–autonomous mechanism for Mtmr2, we analyzed for additional interactors of Mtmr2 by yeast two-hybrid screening (Previtali et al., 2003). Using full-length rat *Mtmr2* cDNA as a bait and a rat peripheral nerve cDNA library, we repeatedly identified Dlg1/SAP97. To provide further evidence that Mtmr2 interacts with Dlg1/SAP97, we performed coimmunoprecipitation experiments on COS-7 cells that were transiently cotransfected with Myc-tagged Mtmr2 and Dlg1/SAP97. When lysates were immunoprecipitated with anti-SAP97 antibody and immunoblotted using anti-Myc antibody, the Mtmr2 protein was revealed (Fig. 6 C). In the converse experiment, when Mtmr2 was immunoprecipitated with an anti-Myc antibody and immunoblotted using anti-SAP97 antibody, SAP97 was revealed (Fig. 6 C′). Conversely, Mtmr2 does not coimmunoprecipitate with discs large 3 (Dlg3), another member of the MAGUK family of proteins containing PDZ domains (unpublished data).

Immunohistochemistry on rat sciatic nerve detected Dlg1/SAP97 in the cytoplasm of myelin-forming and non–myelin-forming Schwann cells, but not in axons (Fig. 6, D–I). In teased sciatic nerve fibers from normal mice, Dlg1/SAP97 staining was enriched in microvilli, which are fingerlike extensions of Schwann cell membrane filling the nodal gap; in the paranodes; and in the Schmidt-Lantermann incisures (Fig. 6, M–O; and not depicted). A similar pattern of staining for MTMR2 was revealed on longitudinal sections of human sural nerves when we used either anti–human MTMR2 or anti–rat Mtmr2. To confirm colocalization of Dlg1/SAP97 and Mtmr2, we double stained longitudinal sections of normal human nerves, where Mtmr2 antibodies produce specific signals (see Expression analysis in *Mtmr2*-null sciatic nerves section). Fig. 6 (J–L) shows that Dlg1/SAP97 and Mtmr2 colocalize in the noncompact myelin cytoplasmic spaces, including the paranodes.

To determine whether loss of Mtmr2 might interfere with the expression or localization of Dlg1/SAP97, we stained transverse sections and teased fibers from sciatic nerves of *Mtmr2*-null mice. Although transverse sections did not show altered intensity or location of Dlg1/SAP97 in mutant nerves, teased fiber analysis revealed that the normal enrichment of Dlg1/SAP97 staining in nodes and paranodes was much less evident in *Mtmr2*-null nerves (Fig. 6, compare M–O with P–R). Western blot analysis showed slightly decreased levels of Dlg1/SAP97 in sciatic nerves from *Mtmr2*-null animals, as compared with normal nerves. When β-tubulin was used to normalize the

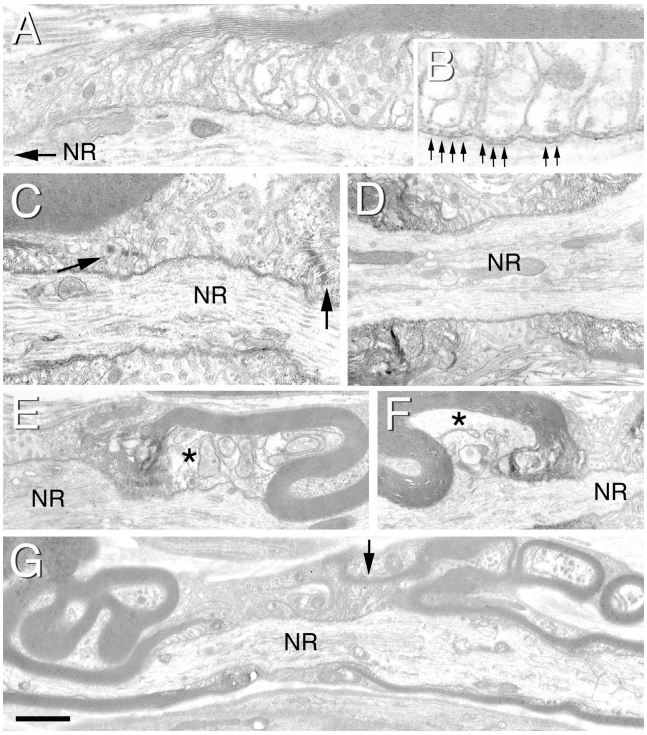

Figure 7. **Ultrastructure of the node of Ranvier.** (A) Paranodal region of a sciatic nerve fiber from *Mtmr2*-null mouse showing normal paranodal loops and basal lamina. Arrow points toward the node of Ranvier (NR). (B) The septate-like junctions (arrows) between paranodal loops of Schwann cell membrane and the axolemma are well-formed and well-preserved. (C) Arrows indicate electron-dense autotypic adherens junctions between paranodal loops of Schwann cell membrane that are in register. (C and D) The gap substance, microvilli, and basal lamina of the node of Ranvier are normal in *Mtmr2*-null nerves. (E–G) Recurrent loops and myelin outfolding originate from the paranodal region that is near the junction between the compact and noncompact myelin (arrow in G). (E and F) Asterisks mark vesicular invaginations of Schwann cell ad-axonal membrane into the axoplasm, which resemble axon–Schwann cell networks. (A–G) The position of the node of Ranvier (NR) is indicated in each section. Bar: (A) 0.3 μm; (B) 0.1 μm; (C and D) 0.5 μm; and (E–G) 1 μm.

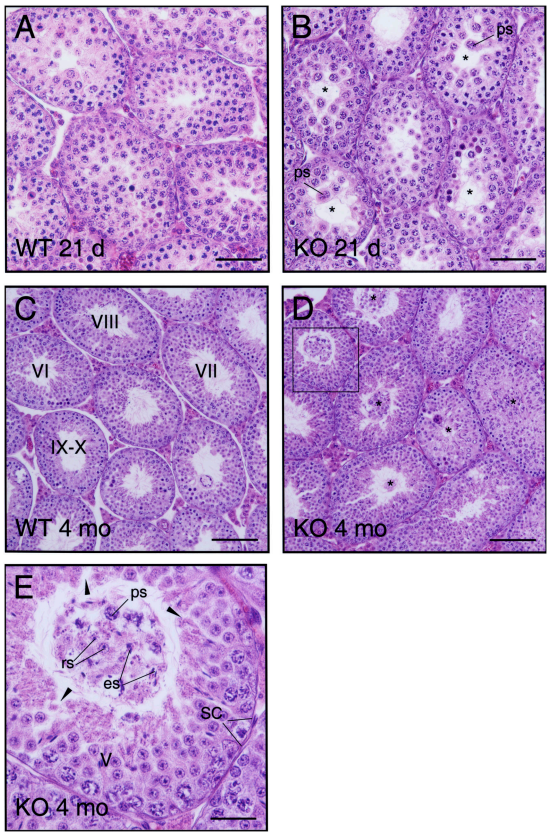

Figure 8. ***Mtmr2*-null mice manifest loss of germ cells from the seminiferous epithelium.** Micrograph of a cross section of a normal (A) or *Mtmr*-null (B) testis at 21 d old. In several mutant tubules (B and D, asterisks), pachytene spermatocytes (ps, E) are detaching from the epithelium. Virtually no round spermatids are detected in these abnormal tubules, as compared to the control. Micrograph of a cross section of a normal (C) and a mutant (D and E, knockout [KO]) testis at 4 mo old. Roman numerals (C) denote the different stages of the epithelial cycle. In several mutant tubules (D, asterisks), meiotic (E, ps) and postmeiotic germ cells (round and elongating spermatids) are shedding from the epithelium and entering the lumen. The boxed area (D), shown magnified (E), is a tubule at stage V of the epithelial cycle. This micrograph (E) clearly illustrates the presence of pachytene spermatocytes (ps), round spermatids (rs), and elongate spermatids (es) in the lumen. Arrowheads depict damaged epithelium. SC, Sertoli cell. Bars: (A and B) 40 μm; (C and D) 100 μm; (E) 20 μm.

relative amount of proteins, this difference was not statistically significant (Fig. 6 B and not depicted).

Ultrastructure of the node of Ranvier

To better understand how myelin outfolding occurs and affects the region surrounding the node of Ranvier, we examined its ultrastructure. Although the nodal gap was slightly longer in *Mtmr2*-null nerves (1.3 ± 0.03(34) vs. 1.1 ± 0.05(19) μm, $P < 0.005$; Figs. 4 D or 7 C), the node appeared otherwise normal. The gap substance, microvilli, and overlying basal lamina, as well as the osmophilic undercoating of nodal axolemma, appeared similar in null and control longitudinal sections (Fig. 7, C and D). Also, the paranodal loops were normally organized, with autotypic electron-dense adherens junctions in register (Fig. 7, A and C), and made normal septate-like junctions with axons (Fig. 7 B) in null nerves. The only obvious abnormality was that most null paranodes had contiguous myelin outfolds or recurrent loops that almost always originated near the junction between compact myelin and noncompact paranodal loop cytoplasm (Fig. 7, E–G). In addition, adjacent to 3 out of 17 *Mtmr2*-null nodes, there were membranous extrusions of various lengths into the axoplasm, containing complex, vesicular internal structures reminiscent of axon–Schwann cell networks (Fig. 7, E and F; Gatzinsky et al., 2003).

Impaired spermatogenesis in *Mtmr2*-null mice

Given the report of azoospermia in CMT4B1 (Laporte et al., 2003), we analyzed testes from *Mtmr2*-null mice at 3 wk and 4 mo old. At 3 wk, some tubules displayed signs of premature germ cell loss from the seminiferous epithelium (Fig. 8, A and B); at 4 mo, many tubules were devoid of elongating/elongate spermatids (Fig. 8, C and D). At higher magnification, spermatids and spermatocytes were found in the lumen of most tubules from mutant testes. In normal mouse testis, no germ cells were found in the lumen except for fully developed spermatids (spermatozoa) at stage VIII of the epithelial cycle (Fig.

8, E vs. C). These data suggest that adhesion between Sertoli and germ cells in the seminiferous epithelium was damaged by the loss of Mtmr2.

Discussion

Mtmr2 (−/−) mice model CMT4B1

Mtmr2-null mice reproduce the demyelinating neuropathy of CMT4B1 and demonstrate defects in spermatogenesis, thus providing the first model for the human pathology and indicating that *MTMR2* mutations in CMT4B1 operate through loss of function. Myelin outfoldings are observed in mutant sciatic nerves by P28. With age, myelin outfoldings and infoldings increase in number and complexity, are more pronounced in distal nerves, and very closely resemble those described in CMT4B1 patients. Here, we exploit the mouse model to demonstrate that the two to five typical satellite fibers, or even fibers invading the central axon, represent recurrent loops from the central fiber. When observed in longitudinal sections, the loops arise predominantly at the level of paranodes, and may reflect all the way back to the Schwann cell nucleus. Both sensory and motor nerves have these abnormalities in *Mtmr2* (−/−) mice, accounting for the combined motor and sensory symptoms and signs of CMT4B1. Finally, early signs of axonal degeneration are detected in nerves from 6-mo-old animals. Interestingly, we noted several paranodal axon–Schwann cell networks in *Mtmr2*-null nerves that may be associated with early axonal degenerative changes in other mutant mice (Gatzinsky et al., 2003).

Overall, *Mtmr2*-null mice do not display a neuropathy as severe as that of human CMT4B1. A significant number of null mice are not born, but we have not established whether neuropathy contributes to their death. Most surviving mutant mice manifest no signs of tremor or functional disability to 6 mo old; possibly the *Mtmr2*-null phenotype will be more severe at older ages. Alternatively, functional redundancy or compensation by other members of the MTMR family may account for the less severe phenotype. Mtm1 and Mtmr2 are both detected throughout the cytoplasm of Schwann cells, raising the possibility of redundant function. In addition, both are thought to recognize PtdIns3,5P_2 as a substrate (see Putative molecular pathogenesis of CMT4B1 section). In contrast, there was no qualitative change in the pattern of expression of Mtm1 and Mtmr1 in null versus control sciatic nerves, which would suggest compensation. A quantitative determination of *Mtm1* and *Mtmr1* mRNA and protein levels in null nerves will be required to strengthen this conclusion. In any case, these data support the possibility that redundant Mtm1 function may more effectively rescue Mtmr2 deficiency in mice than in humans, explaining the less severe phenotype.

The paranodal phenotype of *Mtmr*2-null nerves is reminiscent of the myelin alterations described in MAG-null nerves, the spinal roots of the cat, and in conditional *Nf2*-null nerves. MAG-null nerves have axonal atrophy that is thought to produce secondary redundant loops of myelin at the paranode (Yin et al., 1998). We did not observe obvious changes in axonal diameter in our mice. Myelin remodeling in perinatal cat spinal roots also shows multiple satellite recurrent loops with some invaginating loops, predominantly at paranodes (for review see Berthold and Nilsson, 2002). However, remodelling is much less evident during development in rodents than in cats, and we have not observed myelin debris at *Mtmr2*-null nodes of Ranvier—myelin breakdown products are characteristic in cat myelin remodeling. *Nf2*-null nerves also manifest myelin outfolding (Giovannini et al., 2000). Nf2/merlin is a member of the ezrin/radixin/moesin family of proteins, and is located in Schwann cell microvilli (Poliak and Peles, 2003). Although not strictly analogous, these observations emphasize that myelin remodeling around the node of Ranvier is important, and our data suggest that Mtmr2 regulates it.

Impaired spermatogenesis in *Mtmr2*-null mice

Mtmr2-null mice also display defects in spermatogenesis, confirming the importance of Mtmr2 in testis. A CMT4B1 patient had been reported with azoospermia (Laporte et al., 2003). Moreover, *Mtmr2* expression is significantly enriched in testis (Li et al., 2000). Finally, mice lacking Mtmr5, a catalytically inactive phosphatase, showed impaired spermatogenesis and azoospermia, further emphasizing the importance of the MTMR family in the testis (Firestein et al., 2002). Of note, *Mtmr2* expression rises as junctions between Sertoli and germ cells are formed in vitro (Li et al., 2000).

Several types of junctions maintain proper architecture of the seminiferous epithelium, in which movements of germ cells occur during spermatogenesis. Occludens junctions such as inter–Sertoli cell tight junctions, and anchoring (adherens) junctions such as basal ectoplasmic specializations, are important for an integral blood–testis barrier (Mruk and Cheng, 2004). Anchoring and gap junctions are involved in the cell–cell and cell–matrix interactions and communications. Loss of Mtmr2 disrupts anchoring junctions between Sertoli and germ cells, because elongating and round spermatids, along with spermatocytes, were found in the lumens of most seminiferous tubules of *Mtmr2*-null mice at 4 mo old. Consistent with premature depletion of germ cells from the epithelium, testicular weight and size were reduced by as much as 50% in *Mtmr2*-null mice at 4 mo old. These findings also fit with recent data that implicate intracellular phosphoprotein content in anchoring junction dynamics in the testis (Cheng and Mruk, 2002).

Mtmr2 interacts with Dlg1

We provide evidence that Mtmr2, with a PDZ-binding domain, interacts with Dlg1/SAP97, which carries three PDZ domains. Dlg1/SAP97 is a scaffolding molecule, belonging to the MAGUK protein family (Humbert et al., 2003). It has been detected in septate junctions (in *Drosophila melanogaster*) and apical junctions (in *Caenorhabditis elegans*), and in brain synapses and the lateral membrane of epithelial cells, where adherens junctions are located (in vertebrates; Knust and Bossinger, 2002; Lee et al., 2002). Loss of *D. melanogaster dlg* function produces abnormalities in septate junction formation, cell adhesion, and polarity (Humbert et al., 2003).

Myelin-forming Schwann cells are polarized both radially—in the basal lamina (ab-axonal region), the compact myelin, and the Schwann cell membrane facing the axon (adaxonal region)—and longitudinally—in the node, paranodes, juxtaparanodes, and internode. Microvilli from adjacent Schwann cells are linked by tight junctions at the node. Paranodal loops from Schwann cells contact the axolemma through septate-like junctions. Adjacent loops are also linked by tight, adherens, and gap junctions. Schwann cell polarity, therefore, depends on several types of junctions (Poliak and Peles, 2003). In nerves, we detected Dlg1/SAP97 in the cytoplasm of all Schwann cells. It is enriched in the cytoplasmic spaces of noncompact myelin, such as Schmidt-Lantermann incisures and paranodes, as well as in microvilli. This fits with a function for Dlg1/SAP97 in Schwann cell polarity or junctions.

Putative molecular pathogenesis of CMT4B1

We propose a Schwann cell–autonomous mechanism for *Mtmr2*-null defects based on three observations: (1) myelin outfoldings are obvious and arise predominantly at paranodes; (2) Mtmr2 interacts with Dlg1/SAP97, a scaffolding molecule detected in Schwann cells but not in axons, whose expression is enriched in paranodes/microvilli of wild-type, but not *Mtmr2* (−/−) fibers; and (3) conditional ablation of *Mtmr2* in Schwann cells phenocopies the nerve abnormalities of *Mtmr2*-null mice.

The morphological and immunohistochemical data point to a mechanism originating near the node of Ranvier, and the substrate of Mtmr2 and the genetics of Dlg1 homologues implicate membrane homeostasis. Thus, one simple possibility is that disruption of Mtmr2–Dlg1 interaction dysregulates membrane homeostasis at the paranode. Myelin folds first appeared in our mice between 3 and 4 wk after birth, a time in rodent sciatic nerve when most myelin sheaths are almost fully spiralled and compacted, and are elongating from 200 μm to 1 mm in length (Webster, 1971). Bulk lipid and protein addition likely occur at the trailing edge of the myelin sheath from its outer leaflet (Hendelman and Bunge, 1969; Gould, 1977). Clearly, membrane addition at the trailing edge needs to be progressively balanced by appropriate membrane recovery/destruction at the forward or lateral edge in order to achieve a stable volume of sheath. This volume is dynamically maintained. Mature sheaths actively incorporate label in autoradiographic studies (Hendelman and Bunge, 1969) and can respond acutely to limb elongation with internode elongation (Hara et al., 2003). Paranodes do not contain machinery for membrane synthesis (markers of Golgi are not detected; Scherer, S., personal communication) but they do have clathrin-coated pits, endosomes, and lysosomes (Notterpek et al., 1997; Trapp, B.D., personal communication), the appropriate organelles for endocytic recycling and destruction of membrane.

Strong evidence links Mtmr2/Dlg1 to membrane homeostasis. *D. melanogaster* Dlg associates with endosomes, and Dlg1/SAP97 promotes vesicular trafficking to plasma membrane (Lee et al., 2003). Moreover, the putative substrate of Mtmr2, PtdIns3,5P_2 (Berger et al., 2002, 2003; Tsujita et al., 2004), regulates the late endocytic pathway and mediates Mtmr2 binding to vacuoles (Berger et al., 2003). The family member Mtm1 regulates endocytosis in worm (Dang et al., 2004), perhaps through late endosomal trafficking where it down-regulates PtdIns(3,5)P_2 levels (Tsujita et al., 2004). Interestingly, vacuoles have been detected in muscles of mice lacking Mtm1 and in Sertoli cells of mice lacking Mtmr5 (Firestein et al., 2002; Buj-Bello et al., 2003). By analogy, Mtmr2 could regulate membrane trafficking and cycling at paranodes, being recruited and locally concentrated by Dlg1/SAP97. Loss of Mtmr2/Dlg1 would tip the equilibrium toward membrane excess and myelin outfolding at the paranodes.

Alternatively, loss of Mtmr2/Dlg1 function could disrupt structural elements in the paranodal architecture, thereby producing local myelin alterations. However, in *Mtmr2*-null fibers, the adherens junctions and septate-like junctions around the node appear normal. Finally, disruption of Mtmr2/Dlg1 could dysregulate membrane addition (Lee et al., 2003) at the trailing edge of myelin (both Mtmr2 and Dlg1 are detected there) and secondarily produce myelin alterations at the paranode. Further experiments are underway to test these alternative models, and to understand how myelin alterations at the paranodes specifically produce nerve dysfunction.

Materials and methods

Generation of *Mtmr2*-null mice

pFlrt-1 vector, including *lox-P* sites, *FRT*-flanked neomycin resistance gene (*neo*), and *PGK-TK* was used to target *Mtmr2*. A 2-kb short arm was amplified from an *Mtmr2* BAC clone (CITB library, Research Genetics; Bolino et al., 2002) and inserted into the BstI site, a 7-kb-long arm was inserted between SalI and NotI sites, and a 600-bp BamHI fragment including exon 4 was inserted between *lox-P* sites in pFlrt-1 (provided by P.C. Orban, University of British Columbia, Vancouver, British Columbia, Canada; Fig. 1 A).

After electroporation of TBV2 embryonic stem cells (129S2/SvPas in origin) and G418/gancyclovir plus/minus selection, 200 clones were screened by Southern blot analysis. Digestion with KpnI and an exon 4 probe revealed two bands of 13 kb (wild type) and of 15 kb (Fig. 1 B, neo). Digestion with HindIII and a probe containing exons 6 and 7 revealed two bands of 8 kb (wild type) and 10 kb (neo). Two of seven correctly targeted clones were injected into C57BL6 blastocysts (Core Facility for Conditional Mutagenesis San Raffaele/Telethon Transgenic Service) to obtain transmission of the floxed allele through the germline.

Heterozygous *Mtmr2* (fl/+) animals were crossed with CMV-Cre transgenic mice to excise exon 4 (Fig. 1 A) and generate heterozygous *Mtmr2*-null (+/−) animals; these animals were crossed to generate homozygous *Mtmr2*-null (−/−) mice. Null mice generated from the two different embryonic stem cell clones manifested identical morphological and expression phenotypes in sciatic nerves at 1 and 2 mo old. All experiments involving animals were performed in accordance with Italian national regulations and covered by experimental protocols reviewed by local Institutional Animal Care and Use Committees.

PCR analysis

Genotype analysis of tail genomic DNA used primer pairs C and B (Fig. 1 A, 460-bp wild-type band and 500-bp floxed band) and A and D (no wild-type band and 1-kb floxed band).

RT-PCR was performed as described previously (Bolino et al., 2002) using 30 cycles of amplification. A primer designed on the 5′ UTR was used for RT-PCR analysis in combination with several reverse primers that recognize exons 3, 4, 7, 9, and 10. A primer that recognizes exon 2 was used in combination with reverse primers that recognize exon 13 or the 3′ UTR to check for the 3′ end of the *Mtmr2* mRNA.

Gait analysis

Footprint analysis was performed on 9 *Mtmr2*-null mice and 11 age-matched controls at 6 mo old. Ink was applied to the back paws, and the mice walked forward on white paper for 110 cm in a 7-cm-wide alley.

Five sequential steps from three trials were used to determine stride length (distance between two consecutive left or right prints) and base (distance from a left print to the next right print or vice versa). The center of the print was defined as the plantar cushion underlying the metatarso-phalangeal joint. Each measure was corrected for the body length, which was determined from the neck to the insertion of the tail. Analysis of variance with repeated measures was used for data analysis (SAS/STAT and StatView).

Electrophysiology

8 *Mtmr2*-null and 17 control mice were analyzed at 6 mo old. Mice were anesthetized with trichloroethanol, 0.02 ml/g of body weight, and placed under a heating lamp to avoid hypothermia. The sciatic nerve motor conduction velocity was obtained with steel monopolar needle electrodes: a pair of stimulating electrodes was inserted subcutaneously near the nerve at the ankle; and a second pair of electrodes was placed at the sciatic notch, to obtain two distinct sites of stimulation, proximal and distal, along the nerve. The compound motor action potential was recorded with an active electrode inserted in muscles in the middle of the paw and a reference needle in the skin between the first and second digits.

Histological analysis and electron microscopy

Semithin morphological analysis of sciatic, quadriceps, saphenous, and digital nerves of *Mtmr2* (−/−) animals and control littermates was performed as described previously (Wrabetz et al., 2000). The proportion of fibers with myelin outfoldings was determined in 500 fibers observed in three random microscopic fields from nerves of two animals at 1, 2, 4, and 6 mo old. The proportion of fibers containing three or more satellite loops was calculated as the percentage of fibers showing outfoldings. Ultrathin morphological analysis of sciatic nerves was conducted as reported previously (Wrabetz et al., 2000). For morphological analysis, three to five animals were evaluated at each time point in most cases. The origin of outfoldings was determined in ultrathin longitudinal sections. All nodes of Ranvier from 27 grids from three animals per genotype were photographed at 7,000×. The nodal gap was measured and the number of nodes associated with outfoldings/loops (containing axoplasm contiguous with the main axon) within 10 μm of a paranode were counted. The same grids were scanned for internodal segments longer than 200 μm and not flanked by a paranode, and the proportion containing outfolds/loops (as defined above) was determined.

Testes were fixed in Bouin's fixative for 12–24 h, dehydrated, and embedded in paraffin. 5-μm-thick sections were processed for hematoxylin and eosin staining and mounted for microscopy using a BX 40 microscope (Olympus). Images were captured with a digital camera (model DP 70; Olympus) interfaced with an HP Vectra VL800 Workstation.

Antibodies

Rabbit polyclonal anti-Mtmr2 antibodies have been described previously (Previtali et al., 2003). The following antibodies were used for immunohistochemistry: rabbit polyclonal anti–NF-L (CHEMICON International); rabbit polyclonal anti–NF-H (CHEMICON International); rabbit polyclonal anti-SAP97 (Affinity BioReagents, Inc.); mouse monoclonal anti-Glial fibrillary acidic protein (CHEMICON International); mouse monoclonal anti-S100β (Sigma-Aldrich); mouse monoclonal anti-Caspr (provided by E. Peles, Weizmann Institute of Science, Rehovot, Israel); and rabbit polyclonal anti-Mtm1 and anti-Mtmr1 (provided by A. Buj-Bello and J. Laporte, Institut de Génétique et de Biologie Moléculaire et Cellulaire, Illkirch, France). The specificity of the last two antibodies was characterized by Western blot analysis on COS-7 cells overexpressing either Mtm1 or Mtmr1 and using cells derived from *Mtm1* knockout mice. For Western blot analysis on sciatic nerve homogenates, the following antibodies were used: mouse monoclonal anti–β-tubulin (Sigma-Aldrich) antibody; mouse monoclonal anti-MAG antibody (provided by R. Quarles, National Institute of Neurological Disorders and Stroke, Bethesda, MD); mouse monoclonal anti-P0 antibody (provided by J.J. Archelos, Karl-Franzens University, Graz, Austria); mouse monoclonal anti–PMP-22 (provided by U. Suter, Institute of Cell Biology, ETH Zurich, Zurich, Switzerland); rabbit polyclonal anti-SAP97; mouse monoclonal anti-SAP97 (StressGen Biotechnologies); and rabbit polyclonal anti–NF-L. Secondary antibodies included fluorescein (FITC)- or rhodamine (TRITC)-conjugated goat anti–mouse or rabbit IgG (Southern Biotechnology Associates, Inc.) or peroxidase-conjugated goat anti–mouse or rabbit IgG (DakoCytomation).

Immunohistochemistry and confocal microscopy

Immunofluorescence on cryosections and cell cultures was performed as described previously (Previtali et al., 2003) and examined with confocal (model MRC 1024; Bio-Rad Laboratories) or fluorescent microscopy (model BX; Olympus). For immunohistochemistry, sciatic nerves were removed and rapidly snap-frozen in liquid nitrogen, either unfixed or previously fixed in buffered 4% PFA. For teased fiber preparation, sciatic nerves were removed, fixed on ice in freshly prepared buffered 4% PFA for 30 min, and washed three times in PBS. Then the nerves were placed in a petri dish with cold PBS, the perineurium was removed, and segments were subdivided with fine needles into fine fascicles of nerve fibers. Teased fibers were then dried on a glass slide and stored at 20°C for immunohistochemistry. Slides were immersed in cold acetone for 1 min, rehydrated with PBS, and then blocked at room temperature for 2 h in 5% fish skin gelatin containing 0.5% Triton X-100 in PBS. Slides were incubated overnight at 4°C with primary antibodies. The slides were washed in PBS and incubated with appropriate secondary antibodies (Jackson ImmunoResearch Laboratories) and mounted with Vectashield (Vector Laboratories).

Yeast two-hybrid analysis, cell culture, immunoprecipitation, and Western blot analysis

A yeast two-hybrid screening was performed using a 1,710-bp ORF of rat *Mtmr2* cDNA to encode the bait fused to the GAL4 binding domain (Previtali et al., 2003). A rat sciatic nerve cDNA library cloned into the pACTII vector, carrying the GAL4 activating domain (provided by P. Brophy and D. Sherman, University of Edinburgh, Edinburgh, UK), was used to perform a sequential transformation of yeast strain Y190 (CLONTECH Laboratories, Inc.). 37 out of 118 positive clones contained Dlg1/SAP97. Screening with a fetal brain cDNA library never revealed Dlg1 (Previtali et al., 2003).

Cell transfection and coimmunoprecipitation were performed as described previously (Previtali et al., 2003) with the following vectors and antibodies: rat SAP97 cDNA in a GW1-CMV vector (provided by M. Passafaro, Dulbecco Telethon Institute and CNR Institute of Neuroscience, Milan, Italy); full-length rat *Mtmr2* cDNA ligated into pCMV3B (Stratagene), in frame with an NH_2-terminal Myc tag; anti-SAP97 antibody (for immunoprecipitation); rabbit polyclonal anti-SAP97 antibody; and mouse anti-Myc (Santa Cruz Biotechnology, Inc.; for Western blot). For the converse experiment, the following vectors and antibodies were used: rat SAP97 cDNA in pCMV2B (Stratagene), in frame with an NH_2-terminal Flag tag; *Mtmr2* cDNA in pCMV3B, as above; anti-Myc (for immunoprecipitation); anti-Myc and monoclonal anti-SAP97 (StressGen Biotechnologies) or anti-Flag (Stratagene; for Western blot).

Immunoprecipitation of Mtmr2 was performed on tissue homogenates (lysis buffer Igepal 0.5%; Wrabetz et al., 2000) as described above using 4 mg of brain lysate. Immunoprecipitation was necessary to concentrate endogenous proteins, which are expressed at low levels, as shown for MTM1 (Buj-Bello et al., 2003). Cleared lysates from sciatic nerves (independent homogenates from three mutant mice) were then immunoblotted and densitometry was performed to detect PMP-22, P0, MAG, NF-L, and Dlg1 as normalized by β-tubulin in Western blot analysis (Wrabetz et al., 2000).

Image analysis

Micrographs were digitalized using a scanner (Arcus 2; AGFA) and figures were prepared using Adobe Photoshop 7.0.

We thank Cinzia Ferri and Simona Occhi for help with embryonic stem cells and teased fiber preparation; Anna Buj-Bello, Jocelyn Laporte, Patrizia D'Adamo, Vania Broccoli, Antonio Malgaroli, Anthony Monaco, Steve Pfeiffer, and Robert Gould for advice and critical discussion; Paul Orban for the pFlrt-1 vector; Diane Sherman and Peter Brophy for the rat peripheral nerve cDNA library; and Elior Peles, Juan J. Archelos, Ueli Suter, and Richard Quarles for antibodies.

This study was supported by grants from Telethon (to A. Bolino, S.C. Previtali, M.L. Feltri, and L. Wrabetz); National Institutes of Health (NIH; grants NINDS NS41319 and NS45630 to M.L. Feltri and L. Wrabetz); Compagnia San Paolo (to A. Bolino); Fondazione Italiana Sclerosi Multipla (to S.C. Previtali); and the Fondazione Mariani (to L. Wrabetz). A. Bolino is a recipient of a Telethon Assistant Scientist Career Award. C.Y. Cheng and D.D. Mruk were supported in part by NIH (grants NICHD U01 HD045908 and U54 HD029990, Project 3).

Submitted: 6 July 2004
Accepted: 5 October 2004

References

Azzedine, H., A. Bolino, T. Taieb, N. Birouk, M. Di Duca, A. Bouhouche, S. Benamou, A. Mrabet, T. Hammadouche, T. Chkili, et al. 2003. Muta-

tions in MTMR13, a new pseudo-phosphatase homologue of MTMR2 and Sbf1, in two families with an autosomal recessive demyelinating form of Charcot-Marie-Tooth disease associated with early-onset glaucoma. *Am. J. Hum. Genet.* 72:1141–1153.

Berger, P., S. Bonneick, S. Willi, M. Wymann, and U. Suter. 2002. Loss of phosphatase activity in myotubularin-related protein 2 is associated with Charcot-Marie-Tooth disease type 4B1. *Hum. Mol. Genet.* 11:1569–1579.

Berger, P., C. Schaffitzel, I. Berger, N. Ban, and U. Suter. 2003. Membrane association of myotubularin-related protein 2 is mediated by a pleckstrin-homology-GRAM domain and a coiled-coil dimerization module. *Proc. Natl. Acad. Sci. USA*. 21:12177–12182.

Berthold, C.H., and R.I. Nilsson. 2002. De- and remyelination in spinal roots during normal perinatal development in the cat: a brief summary of structural observations and a conceptual hypothesis. *J. Anat.* 200:391–403.

Bolino, A., M. Muglia, F.L. Conforti, E. LeGuern, M.A. Salih, D.M. Georgiou, K. Christodoulou, I. Hausmanowa-Petrusewicz, P. Mandich, A. Schenone, et al. 2000. Charcot-Marie-Tooth type 4B is caused by mutations in the gene encoding myotubularin-related protein-2. *Nat. Genet.* 25:17–19.

Bolino, A., V. Marigo, F. Ferrera, J. Loader, L. Romio, A. Leoni, M. Di Duca, R. Cinti, C. Cecchi, M.L. Feltri, et al. 2002. Molecular characterization and expression analysis of *Mtmr2,* mouse homologue of *MTMR2,* the Myotubularin-related 2 gene, mutated in CMT4B. *Gene.* 283:17–26.

Buj-Bello, A., V. Laugel, N. Messaddeq, H. Zahreddine, J. Laporte, J.F. Pellissier, and J.L. Mandel. 2003. The lipid phosphatase myotubularin is essential for skeletal muscle maintenance but not for myogenesis in mice. *Proc. Natl. Acad. Sci. USA.* 99:15060–15065.

Cheng, C.Y., and D.D. Mruk. 2002. Cell junction dynamics in the testis: Sertoli-germ cell interactions and male contraceptive development. *Physiol. Rev.* 82:825–874.

Dang, H., Z. Li, E.Y. Skolnik, and H. Fares. 2004. Disease-related myotubularins function in endocytic traffic in *Caenorhabditis elegans*. *Mol. Biol. Cell.* 15:189–196.

Feltri, M.L., D. Graus Porta, S.C. Previtali, A. Nodari, B. Migliavacca, A. Cassetti, A. Littlewood-Evans, L.F. Reichardt, A. Messing, A. Quattrini, et al. 2002. Conditional disruption of β1 integrin in Schwann cells impedes interaction with axons. *J. Cell Biol.* 156:199–209.

Firestein, R., P.L. Nagy, M. Daly, P. Huie, M. Conti, and M.L. Cleary. 2002. Male infertility, impaired spermatogenesis, and azoospermia in mice deficient for the pseudophosphatase Sbf1. *J. Clin. Invest.* 109:1165–1172.

Gatzinsky, K.P., B. Holtmann, B. Daraie, C.-H. Berthold, and M. Sendtner. 2003. Early onset of degenerative changes at nodes of Ranvier in alpha-motor axons of Cntf (−/−) mutant mice. *Glia.* 42:340–349.

Giovannini, M., E. Robanus-Maandag, M. van der Valk, M. Niwa-Kawakita, V. Abramowski, L. Goutebroze, J.M. Woodruff, A. Berns, and G. Thomas. 2000. Conditional biallelic Nf2 mutation in the mouse promotes manifestations of human neurofibromatosis type 2. *Genes Dev.* 14:1617–1630.

Gould, R.M. 1977. Incorporation of glycoproteins into peripheral nerve myelin. *J. Cell Biol.* 75:326–338.

Hara, Y., T. Shiga, I. Abe, A. Tsujino, H. Ichimura, N. Okado, and N. Ochiai. 2003. P0 mRNA expression increases during gradual nerve elongation in adult rats. *Exp. Neurol.* 184:428–435.

Hendelman, W.J., and R.P. Bunge. 1969. Radioautographic studies of choline incorporation into peripheral nerve myelin. *J. Cell Biol.* 40:190–208.

Houlden, H., R.H. King, N.W. Wood, P.K. Thomas, and M.M. Reilly. 2001. Mutations in the 5′ region of the myotubularin-related protein 2 (MTMR2) gene in autosomal recessive hereditary neuropathy with focally folded myelin. *Brain.* 124:907–915.

Humbert, P., S. Russell, and H. Richardson. 2003. Dlg, Scribble and Lgl in cell polarity, cell proliferation and cancer. *Bioessays.* 25:542–553.

Ikonomov, O.C., D. Sbrissa, K. Mlak, M. Kanzaki, J. Pessin, and A. Shisheva. 2002. Functional dissection of lipid and protein kinase signals of PIKfyve reveals the role of PtdIns3,5-P_2 production for endomembrane integrity. *J. Biol. Chem.* 277:9206–9211.

Knust, E., and O. Bossinger. 2002. Composition and formation of intercellular junctions in epithelial cells. *Science.* 298:1955–1959.

Laporte, J., F. Bedez, A. Bolino, and J.L. Mandel. 2003. Myotubularins, a large disease-associated family of cooperating catalytically active and inactive phosphoinositides phosphatases. *Hum. Mol. Genet.* 12:R285–R292.

Lee, S., S. Fan, O. Makarova, S. Straight, and B. Margolis. 2002. A novel and conserved protein-protein interaction domain of mammalian Lin-2/CASK binds and recruits SAP97 to the lateral surface of epithelia. *Mol. Cell. Biol.* 22:1778–1791.

Lee, O.K., K.K. Frese, J.S. James, D. Chadda, Z.H. Chen, R.T. Javier, and K.O. Cho. 2003. Discs-Large and Strabismus are functionally linked to plasma membrane formation. *Nat. Cell Biol.* 5:987–993.

Li, J.C., E.T. Samy, J. Grima, S.S. Chung, D. Mruk, W.M. Lee, B. Silvestrini, and C.Y. Cheng. 2000. Rat testicular myotubularin, a protein tyrosine phosphatase expressed by Sertoli and germ cells, is a potential marker for studying cell-cell interactions in the rat testis. *J. Cell. Physiol.* 185: 366–385.

Mruk, D.D., and C.Y. Cheng. 2004. Sertoli-Sertoli and Sertoli-germ cell interactions and their significance in germ cell movement in the seminiferous epithelium during spermatogenesis. *Endocr. Rev.* 25:747–806.

Notterpek, L., E.M. Shooter, and G.J. Snipes. 1997. Upregulation of the endosomal-lysosomal pathway in the trembler-J neuropathy. *J. Neurosci.* 17: 4190–4200.

Odorizzi, G., M. Babst, and S.D. Emr. 1998. Fab1p PtdIns(3)P 5-kinase function essential for protein sorting in the multivesicular body. *Cell.* 95: 847–858.

Poliak, S., and E. Peles. 2003. The local differentiation of myelinated axons at nodes of Ranvier. *Nat. Rev. Neurosci.* 4:968–980.

Previtali, S.C., B. Zerega, D.L. Sherman, P.J. Brophy, G. Dina, R.H. King, M.M. Salih, L. Feltri, A. Quattrini, R. Ravazzolo, et al. 2003. Myotubularin-related 2 protein phosphatase and neurofilament light chain protein, both mutated in CMT neuropathies, interact in peripheral nerve. *Hum. Mol. Genet.* 12:1713–1723.

Quattrone, A., A. Gambardella, F. Bono, U. Aguglia, A. Bolino, A.C. Bruni, M.P. Montesi, R.L. Oliveri, M. Sabatelli, O. Tamburrini, et al. 1996. Autosomal recessive hereditary motor and sensory neuropathy with focally folded myelin sheaths: clinical, electrophysiologic, and genetic aspects of a large family. *Neurology.* 46:1318–1324.

Senderek, J., C. Bergmann, S. Weber, U.P. Ketelsen, H. Schorle, S. Rudnik-Schoneborn, R. Buttner, E. Buchheim, and K. Zerres. 2003. Mutation of the *SBF2* gene, encoding a novel member of the myotubularin family, in Charcot-Marie-Tooth neuropathy type 4B2/11p15. *Hum. Mol. Genet.* 12: 349–356.

Suter, U., and S.S. Scherer. 2003. Disease mechanism in inherited neuropathies. *Nat. Rev. Neurosci.* 4:714–726.

Tsujita, K., T. Itoh, T. Ijuin, A. Yamamoto, A. Shisheva, J. Laporte, and T. Takenawa. 2004. Myotubularin regulates the function of the late endosome through the gram domain-phosphatidylinositol 3,5-bisphosphate interaction. *J. Biol. Chem.* 279:13817–13824.

Webster, H.D. 1971. The geometry of peripheral myelin sheaths during their formation and growth in rat sciatic nerves. *J. Cell Biol.* 48:348–367.

Wrabetz, L., M. Feltri, A. Quattrini, D. Inperiale, S. Previtali, M. D'Antonio, R. Martini, X. Yin, B. Trapp, L. Zhou, et al. 2000. P_0 glycoprotein overexpression causes congenital hypomyelination of peripheral nerves. *J. Cell Biol.* 148:1021–1033.

Yin, X., T.O. Crawford, J.W. Griffin, P. Tu, V.M. Lee, C. Li, J. Roder, and B.D. Trapp. 1998. Myelin-associated glycoprotein is a myelin signal that modulates the caliber of myelinated axons. *J. Neurosci.* 18:1953–1962.